increasing temperature is suggestive of an increasing dipole density and a faster polarization process

$$\tau = \tau_0 \exp(U/k_B T) \quad (6)$$

(k_B, Boltzmann constant). A linear regression of log τ versus $1/T$ (Fig. 4B) describes the data quite well, as indicated by the dotted line, and yields $U = 54$ meV (630 K) and $\tau_0 = 84$ ns. For 100 K $\lesssim T \lesssim U$, ε_0 is approximately constant, but for $T \gtrsim U$, the dielectric constant begins to increase rapidly to over 3×10^5 in the ceramic materials at ~400°C (~670 K) (*1*).

Subramanian *et al.* (*1*) speculate that the high dielectric constant of this material is enhanced by its microstructure because of the creation of an effective circuit of parallel capacitors, as found in boundary-layer dielectrics (*15*). The recurring observation of twinned single crystals at very small length scales suggests this as a possible mechanism to create barrier layer capacitances at the twin boundaries, thereby enhancing ε_0.

The origin of the large dipole moments P_0 is still uncertain at this time. Polar domains could be induced by local distortions, due to, for example, symmetrical off-center Ti displacements along the eight <111> directions, as is common in TiO_6-containing compounds. However, it is surprising that, unlike in other stoichiometric titanates, a ferroelectric transition is not observed. Rather, the electric dipoles freeze through a relaxational process; at low temperatures, one observes a relaxor-like slowing down of the dipole fluctuations as evidenced by the dramatic increase in τ and a dramatic decrease in ε_0. A clue to the large dielectric constant comes from its near temperature-independence at high temperatures, which implies that the correlation length does not grow on cooling as in conventional ferroelectrics. Further, it is unusual that the changes in bonding within the TiO_6 octahedron do not distort the structure, as is usually observed in perovskite compounds; the bcc structure persists down to low temperature. At present, these results suggest that the octahedral tilt (Fig. 1) is large enough to accommodate local distortions, thus effectively decoupling the ferroelectric order parameter and the crystal structure. Then, given the bcc structure, which prohibits ferroelectricity on symmetry grounds, the present results are consistent with a geometrical frustration of ferroelectric order (*1*).

References and Notes

1. M. A. Subramanian, Dong Li, N. Duan, B. A. Reisner, A. W. Sleight, *J. Solid State Chem.* **151**, 323 (2000).
2. P. Ramirez *et al.*, *Solid State Commun.* **115**, 217 (2000).
3. R. Singh, R. K. Ulrich, *Electrochem. Soc. Interface* **8**, 26 (1999).
4. B.-G. Kim, S. M. Cho, T.-Y. Kim, H. M. Jang, *Phys. Rev. Lett.* **86**, 3404 (2001).
5. Z. Zeng, M. Greenblatt, M. A. Subramanian, M. Croft, *Phys. Rev. Lett.* **82**, 3164 (1999).
6. D. Bruce, R. A. Cowley, *Structural Phase Transitions* (Taylor & Francis, London, 1981).
7. X. X. Bochu, M. N. Deschizeaux, J. C. Joubert, *J. Solid State Chem.* **29**, 291 (1979).
8. The transport measurements were performed at Lucent Technologies, Bell Labs, 600 Mountain Avenue, Murray Hill, NJ 07974, USA.
9. V. V. Daniel, *Dielectric Relaxation* (Academic Press, New York, 1967), pp. 4–19.
10. C. C. Homes, M. Reedyk, D. A. Crandles, T. Timusk, *Appl. Opt.* **32**, 2972 (1993).
11. D. Y. Smith, in *Handbook of Optical Constants of Solids*, E. D. Palik, Ed. (Academic Press, New York, 1985), pp. 35–68.
12. J. F. Scott, *Phys. Rev. B* **4**, 1360 (1971).
13. S. Tajima *et al.*, *Phys. Rev. B* **43** 10496 (1991).
14. W. W. Porterfield, *Inorganic Chemistry, a Unified Approach* (Academic Press, New York, ed. 2, 1993); A. M. James, M. P. Lord, *Mcmillan's Chemical and Physical Data* (Macmillan, London, 1992); J. E. Huheey, E. A. Keiter, R. L. Keiter, *Inorganic Chemistry: Principles of Structure and Reactivity* (HarperCollins, New York, ed. 4, 1993).
15. C. F. Yang, *Jpn. J. Appl. Phys.* **36**, 188 (1996).

16. We thank D. Buttrey, J. F. Scott, A. W. Sleight, D. Vanderbilt, R. Werner, and P. Woodward for fruitful discussions. The work at Brookhaven was supported by the U.S. Department of Energy under contract no. DE-AC02-98CH10886. The work at MIT was supported by NSF under grant no. DMR0071256 and by the MRSEC Program of NSF under award no. DMR98-08941.

16 April 2001; accepted 26 June 2001

β-Helical Polymers from Isocyanopeptides

Jeroen J. L. M. Cornelissen,[1] Jack J. J. M. Donners,[3] René de Gelder,[2] W. Sander Graswinckel,[1] Gerald A. Metselaar,[1] Alan E. Rowan,[1] Nico A. J. M. Sommerdijk,[3] Roeland J. M. Nolte[1,3]*

Polymerization of isocyanopeptides results in the formation of high molecular mass polymers that fold in a proteinlike fashion to give helical strands in which the peptide chains are arranged in β-sheets. The β-helical polymers retain their structure in water and unfold in a cooperative process at elevated temperatures. The peptide architecture in these polymers is a different form of the β-helix motif found in proteins. Unlike their natural counterparts, which contain arrays of large β-sheets stacked in a helical fashion, the isocyanopeptide polymers have a central helical core that acts as a director for the β-sheet–like arrangement of the peptide side arms. The helical structure of these isocyanopeptide polymers has the potential to be controlled through tailoring of the side branches and the hydrogen-bonding network present in the β-sheets.

The two principal structural elements found in proteins are the α-helix and the β-sheet. In 1993, a new structural motif was discovered, the so-called β-helix, which was first observed in the bacterial enzyme *pectate lyase* (*1*). The β-helical architecture is constructed from polypeptides that are coiled into a large helix, formed by stacks of β-sheets separated by loops. β-Sheet helices are present in the fibrous form of *thransyretin*, which plays an important role in bovine spongiform encephalopathy (BSE) and Creutzfeld-Jacob diseases, type II diabetes, and Alzheimer's disease (*2*), and form the crucial structural elements in insect antifreeze proteins (*3*). We report on synthetic analogs of β-helices (*4*, *5*) that are formed by polymerization of isocyanopeptides (*6*).

Polymers of isocyanides are prepared by a nickel(II)-catalyzed reaction (*6*). They adopt a ~4_1 helical conformation (four repeats per turn) when bulky side groups are present [e.g., poly(*tertiary*-butylisocyanide)] (*7*). In the case of less sterically demanding side chains (*8*, *9*) (e.g., polyphenylisocyanide), the helical backbone slowly uncoils upon standing in solution (*10*). The helix sense of the backbone can be controlled with either optically active monomers or a chiral nickel catalyst (*6*). We describe the polymerization of isocyanopeptides leading to products in which the helical backbone is stabilized by hydrogen bonds between amide groups in parallel side chains (*11*). Each side chain can be regarded as an individual β-strand, and the overall arrangement of the side chains leads to a helical β-sheet–like organization. We prepared a series of polymers derived from L- and D-alanine–containing peptides (Fig. 1A) [see supplementary information (*12*)] to investigate the structural properties of these macromolecules, in particular the hydrogen-bonding patterns.

A β-sheet–like hydrogen-bonding array between stacked peptide strands is present in single crystals of the monomer L-isocyanoalanyl-L-alanine methyl ester (L,L-IAA; Fig. 1B). This results in a characteristic N-H stretching vibra-

[1]Department of Organic Chemistry, [2]Department of Inorganic Chemistry, University of Nijmegen, Toernooiveld 1, 6525 ED Nijmegen, Netherlands. [3]Laboratory for Macromolecular and Organic Chemistry, Eindhoven University of Technology, Post Office Box 513, 5600 MB Eindhoven, Netherlands.

*To whom correspondence should be addressed. E-mail: nolte@sci.kun.nl

tion in the solid state infrared (IR) spectrum of this compound (ν_{NH} = 3279 cm^{-1}), whereas no indication of hydrogen bonding could be observed in chloroform solution (Table 1). Similar results were observed for the other investigated isocyanopeptide monomers. The IR spectra of the polymers all showed N-H stretching vibrations in the range of 3260 to 3300 cm^{-1}, both in solution and in the solid state, implying that they have a structure in which the side chains have a hydrogen-bonding arrangement similar to that found in the crystal structure of L,L-IAA and that this arrangement is preserved in solution. The positions of the amide carbonyl vibrations also clearly indicated their participation in a hydrogen-bonding array (*13*). Further confirmation of the presence of hydrogen bonds came from proton nuclear magnetic resonance (^{1}H NMR) spectroscopy (*14*). All the resonances assigned to the amide protons of the isocyanopeptides were substantially shifted downfield by 1.5 to 2.5 parts per million (ppm) upon polymerization, indicative of very strong hydrogen bonding (Table 1). Both the IR and the ^{1}H NMR spectra were absent of any signals corresponding to amide groups not participating in hydrogen bonds.

The tightly coiled helical organization of the peptide strands, stabilized by the hydrogen bonds, leads to rodlike polymers. In the solid state, these rods are ordered in an orthorhombic fashion as demonstrated by powder x-ray diffraction (PXRD). The diameters of the individual rods were calculated to be 15.8 Å for both L,L-PIAA and L,D-PIAA (Fig. 2). The macromolecular diameter is strongly correlated to the overall helical architecture. The 4_1 helix, which has been established in the past (*6*, *8*, *10*), can be regarded as a spring. Stretching of this "polymeric spring" elongates the polymer backbone and shortens the diameter of the rods. Molecular modeling calculations in combination with NMR studies (see below) revealed that the observed polymer diameters were in agreement with a 4_1 helix having a helical pitch of 4.6 Å and an average spacing between the side chains *n* and (*n* + *4*) of 4.7 Å (Fig. 2). A value of 4.728 Å was found in the crystal structure of L,L-IAA (Fig. 1B).

A lyotropic liquid crystalline phase (Fig. 3A) was observed for all peptide-derived polymers in $CHCl_3$ solution (> 10% w/w) highlighting the rigid rodlike architecture of the polymer. The polyisocyanopeptides could be visualized by atomic force microscopy (AFM) because of the stiffness of the polymer chains, which showed individual molecules with lengths of up to 200 nm for samples prepared by the nickel(II)-catalyzed reaction. Analysis of the AFM micrographs allowed the determination of the average length and consequently the molecular masses of the respective polymers (Fig. 3B) (*15*).

The introduction of an additional amino acid onto the peptide side chain (L,L,L- PIAAA) resulted in a more developed β-helical architecture. It was evident from the IR and ^{1}H NMR data obtained for this tripeptide polymer (Table 1) that both side chain amide functionalities are involved in hydrogen bonding. The well-defined arrangement of the side chains was further confirmed by nuclear Överhauser effect spectroscopy (NOE). The α proton (H-1) of the first alanine residue of the side chain *n* exhibited an NOE with the first amide proton (H-3) and the α proton (H-4) of the second alanine unit of the side chain in the next turn. In addition, NOEs were also observed between H-6 and H-7 and the methyl ester protons (H-9) (Fig. 1C). Calculations showed that such contacts are only possible between stacked side chains in an *n*/(*n* + 4) β-sheet–like organization, as shown in Fig. 2. In this architecture, the polymer backbone acts as a director (*5*) to align the β-sheet side arms in a helical manner. This is a β-helical motif different from that found in naturally occurring proteins and synthetic foldamers (*4*), which contain helical stacks of β-sheets without an aligning central core.

The β-helical conformation of these polymers could be altered by disrupting the hydrogen bonds, in a manner analogous to the denaturation of proteins. This process is best moni-

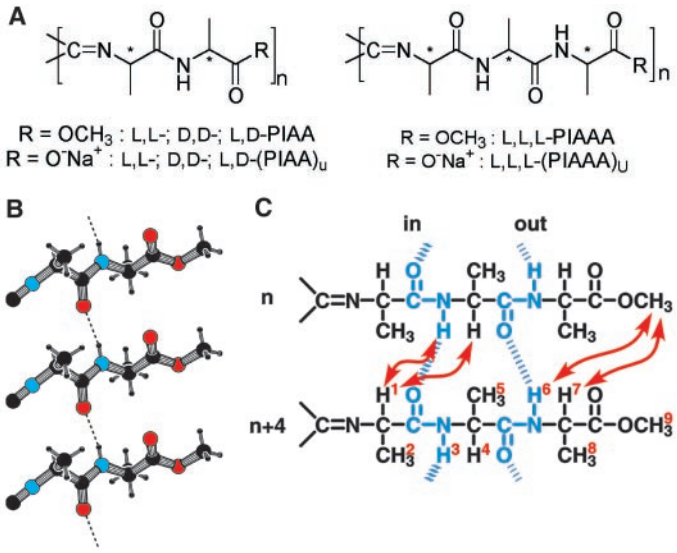

Fig. 1. (**A**) Chemical structures of the β-helical polymers from isocyanopeptides. (**B**) Pluton (*24*) drawing of the crystal structure of L-isocyanoalanyl-L-alanine methyl ester, showing three molecules and the intramolecular hydrogen bonds. Crystal data: $C_8H_{12}N_2O_3$; orthorhombic, space group $P2_12_12_1$; *a* = 4.7281 ± 0.0006 Å; *b* = 9.202 ± 0.002 Å; *c* = 23.792 ± 0.004 Å; *V* = 1035.1 ± 0.3 $Å^3$; *Z* = 4 (deposited at the Cambridge Crystallographic Data Centre under number CCDC 148386). (**C**) NOE interactions in L,L,L-PIAAA between side chains *n* and *n* + 4, which are stacked above each other.

Table 1. Selected IR and ^{1}H NMR data of isocyanopeptides and their polymers.

	Isocyanopeptide				Peptide polymer as methyl ester				Peptide polymer as sodium salt		
	ν_{NH} (KBr) (cm^{-1})	ν_{NH} ($CDCl_3$) (cm^{-1})	ν_{amidI}, ν_{amidII} ($CDCl_3$) (cm^{-1})	δ_{NH} ($CDCl_3$) (ppm)	ν_{NH} (KBr) (cm^{-1})	ν_{NH} ($CDCl_3$) (cm^{-1})	ν_{amidI}, ν_{amidII} ($CDCl_3$) (cm^{-1})	δ_{NH} ($CDCl_3$) (ppm)	ν_{NH} (KBr) (cm^{-1})	ν_{amidI}, ν_{amidII} (KBr) (cm^{-1})	δ_{NH} [$T_{1/2}$]* (D_2O) (ppm)
L,L-IAA	3279	3430†	1688, 1519	6.91	3276	3265	1657, 1532	9.18†	3288‡	1647, 1537	8.8† [>24]
L,D-IAA	3304	3416	1687, 1522	6.97	3280	3252	1657, 1530	9.42	3304‡	1647, 1527	8.3 [>24]
L,L,L-IAAA	3315	3420§	1675, 1511	7.04	3300	3290	1648, 1536	9.50	3305‡	1653, 1528	8.2 [>18]‖
	3285			6.38	3267	3260		7.81			

*Estimated half-life time of H/D exchange in hours. †Split signals; average values are given. ‡Appearing as a shoulder on a larger peak. §In a non–hydrogen-bonded state, only one signal is observed for both N-H vibrations. ‖After 48 hours, a residual broad NH signal remained that we attribute to the nonexchanging inner amide protons. All measurements were performed at room temperature.

tored by examining the changes in the circular dichroism (CD) spectra of the peptide polymers at about 315 nm where the n-π* transitions of the backbone imine subunits occur. The organization of the amide arrays is reflected in the Cotton effects at this wavelength, which are highly sensitive to the environment of the hydrogen bonds. Upon the addition of trifluoroacetic acid (TFA) to L,L,L-PIAAA, the 321-nm CD band gradually decreased, and a new band centered around 360 nm appeared with an isodichroic point at 345 nm (see Web fig. 1) (*12*). These results indicate that the breaking of the hydrogen bonds results in a slow transition of one discrete conformation into another. Variable temperature (VT) ^{1}H NMR experiments indicated that only the outer one of the two hydrogen-bonding arrays ($\delta = 7.81$ ppm, Table 1, Fig. 1C) became disrupted, whereas the inner one remained initially unchanged. In the case of the dipeptide polymers L,L-PIAA and D,D-PIAA, addition of TFA completely destroyed the hydrogen-bonding network, and a less defined macromolecular structure was obtained, as was also indicated by PXRD experiments on the acidified samples, which only showed broad peaks.

Molecular model calculations revealed that the helix of L,D-PIAA is more stable than that of L,L-PIAA. In the latter case, the methyl group of the second alanine unit is in van der Waals contact with the methyl group of the first alanine entity of the next repeating unit, thereby leading to an unfavorable steric interaction. In the case of L,D-PIAA, this methyl group and the proton in the second alanine function are interchanged, and this interaction is then absent (Fig. 2C). We found that the L,D-IAA monomer could be polymerized even without the templating effect of the nickel center, i.e., by adding a small amount of TFA to a solution of this monomer in dichloromethane. This resulted in optically active polymers that had the same chiroptical properties as the polyisocyanopeptides prepared with the help of the nickel(II) catalyst. AFM studies indicated that the thus prepared polymer chains were exceptionally long (up to 5 μm, which corresponds to a molecular mass $>10^6$ daltons; Fig. 3B). Detailed CD studies monitoring the acid-catalyzed polymerization reaction as a function of time revealed sigmoidal conversion curves that suggest that the polyisocyanopeptide chains fold cooperatively into a β-helical conformation (Fig. 4A). The L,L-isomer did not polymerize under the applied conditions, showing the substantial effect of the second chiral center, which is situated six atoms away from the isocyano function, upon the polymerization reaction.

The folding of peptides in water is dictated by a well-defined set of secondary interactions involving hydrogen bonds, van der Waals interactions, and hydrophobic effects. It has been notoriously difficult to achieve well-defined conformations of synthetic oligomers and polymers stabilized by hydrogen bonds in aqueous solution (*4*, *16*–*19*). To investigate whether the present β-helical polymers would retain their structure in aqueous solution, we removed the methyl ester functions in the side chains with base to yield water-soluble polyisocyanopeptides (Fig. 1A). No substantial shifts in the positions of the amide I and II absorption bands were observed after treatment (Table 1), indicating that the amide hydrogen bonds between the side chains remained intact. Strong evidence for the retention of the hydrogen bonds in aqueous solution came from ^{1}H NMR experiments. The exchange of the NH protons for deuterium in D_2O was slow as expected for protons participating in hydrogen bonds (*20*) (Table 1). VT ^{1}H NMR spectroscopy further confirmed the presence of such hydrogen bonds; a shift of the NH resonances toward higher field was observed in D_2O upon increasing the temperature for both L,L- and L,D-$(PIAA)_u$ and L,L,L-$(PIAAA)_u$. NOE spectroscopy experiments on the latter polymer (concentration ~ 40 mM expressed per repeat unit) indicated that several protons in the side chains were in close proximity.

CD spectroscopy was also used to investigate the structural properties of the β-helical polymers in water. The broader spectral window available in this solvent also enabled the amide region of the polyisocyanopeptides to be studied. A negative CD signal was found between 260 and about 400 nm, because of the imine n-π* transitions (Fig. 4), for both L,L- and L,D-$(PIAA)_u$ and L,L,L-$(PIAAA)_u$. The CD bands appearing between 200 and 260 nm can be assigned to the amide groups present in the

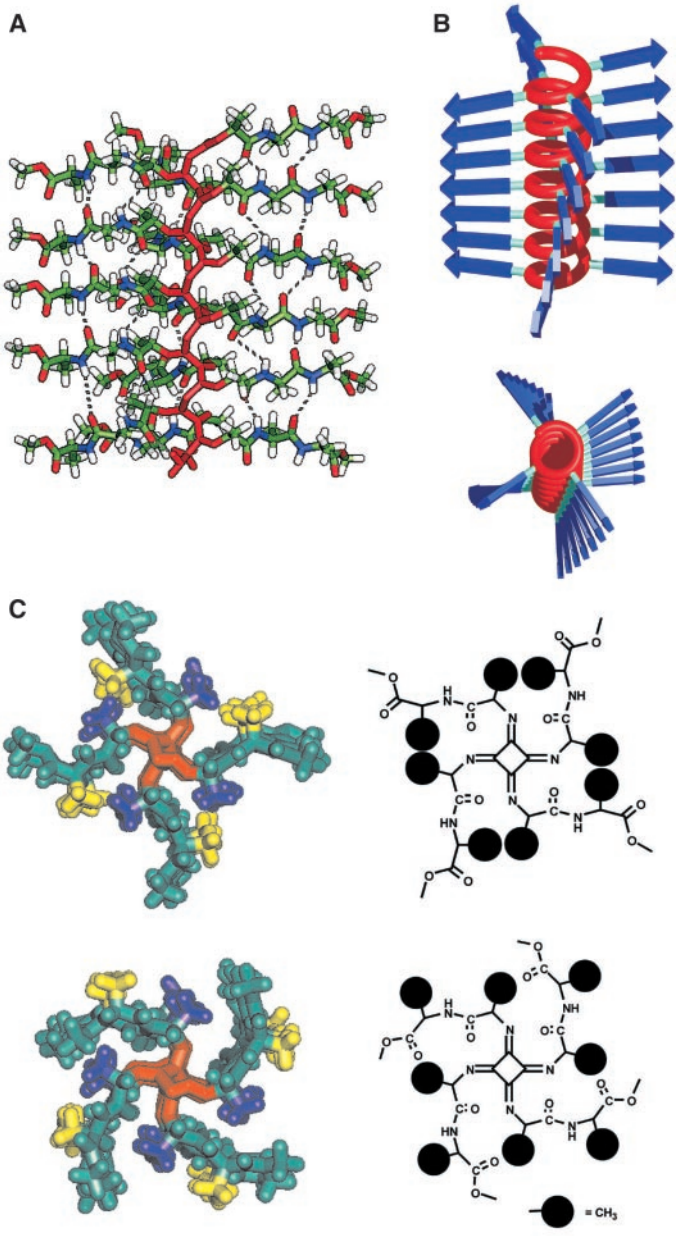

Fig. 2. β-Helical polymers from isocyanopeptides. (**A**) Calculated structure of a 24-residue-long L,L,L-PIAAA chain; the right-handed helical backbone is shown in red, and the dashed lines indicate the hydrogen bonds. One strand of side chains (the one toward the viewer) is not displayed to give a clearer view on the polymeric backbone (CHARMm Version 3.0, Revision 92.0911). (**B**) Schematic model showing the helical backbone (red) and the β-strands (blue). (Top) Side view highlighting the stacked arrangement of the β-strands. (Bottom) Top view. As a result of the helical pitch being smaller than the optimum hydrogen-bonding distance, the β-strands have an offset helical stacking (POV-ray version 3.02). (**C**) Molecular models of L,L-PIAA (top) and L,D-PIAA (bottom) revealing the different configurations of the side chains. In black: schematic drawings showing the difference in steric interactions resulting from the change in side chain configuration.

side chains, and, as expected, these bands were different for the three β- helical polymers. VT-CD experiments showed that high structural order is present at room temperature and below but that this order is lost at elevated temperatures. Dilution studies indicated that the observed CD effects are not the result of aggregation but are inherent to the macromolecular architecture. The observed nonlinear decrease in intensity in the imine region was attributed to the cooperative unwinding of the helical backbone for all β-helical polymers investigated (Fig. 4). This unfolding of the polyisocyanopeptides was found to be irreversible as in the case of proteins; i.e., once unfolded, the helical geometry was not recovered and only local order of the side chains was regained. The observed changes in the spectra in the amide region during the VT experiments also supported the cooperative unwinding of the polymer chains upon increasing temperature. After cooling to 298 K, about 20% of the original intensity was recovered, showing that the helix cannot completely refold into its native state. The behavior was more complex in the case of the tripeptide polymer. The decrease in the amide CD band appeared to be linear with increasing temperature in contrast to the S-shaped curve observed for the CD band of the imines (Fig. 4C). It has been previously proposed that the formation and disruption of hydrogen bonds in β-sheets are complex processes that proceed cooperatively in a direction perpendicular to the strand (*21*, *22*), but they may not be cooperative along the strand direction. It is possible that in the tripeptide polymer, a similar dual mechanism is operative: a noncooperative one on initial heating and a cooperative one on further heating, leading to the observed VT curve at 215 nm. The curve at 290 nm reveals that the unwinding of the helix is an overall cooperative process, linked to the breaking of the inner hydrogen-bonded array.

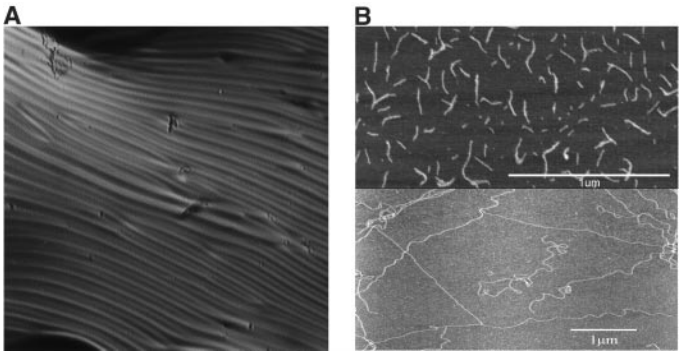

Fig. 3. (**A**) Optical micrograph of a polyisocyanopeptide (L,L-PIAA) solution between crossed polarizers, displaying the characteristic fingerprint texture of a cholesteric phase. The presence of a cholesteric organization in the lyotropic phase was supported by the high specific optical rotation ($[\alpha]_D$) of concentrated solutions compared with those of dilute solutions of the peptide polymers; e.g., for L,L-PIAA $[\alpha]_D = +338°$ [$CHCl_3$, concentration (c) = 0.34 g/dl] versus $[\alpha]_D = -72{,}000°$ ($CHCl_3$, c = 19.4 g/dl). (**B**) (Top) Tapping mode AFM micrograph of L,L-PIAA (shown as an example) prepared by nickel(II)-catalyzed polymerization. From this micrograph, the number-averaged molecular mass (M_n) and polydispersity index (PDI) were calculated to be M_n = 140 kg/mol and PDI = 1.4; the former number corresponds to 760 repeat units. For L,D-PIAA, M_n = 280 kg/mol and PDI = 1.9 were found; for L,L,L-PIAAA, M_n = 290 kg/mol and PDI = 1.6 (*15*). (Bottom) AFM micrograph of L,D-PIAA prepared by acid initiation, displaying polymer chains that are micrometers long (see text). Height analysis of the AFM micrographs revealed polymer diameters in agreement with the x-ray data. Samples were obtained by spin coating a 0.01 g/l solution on freshly cleaved mica.

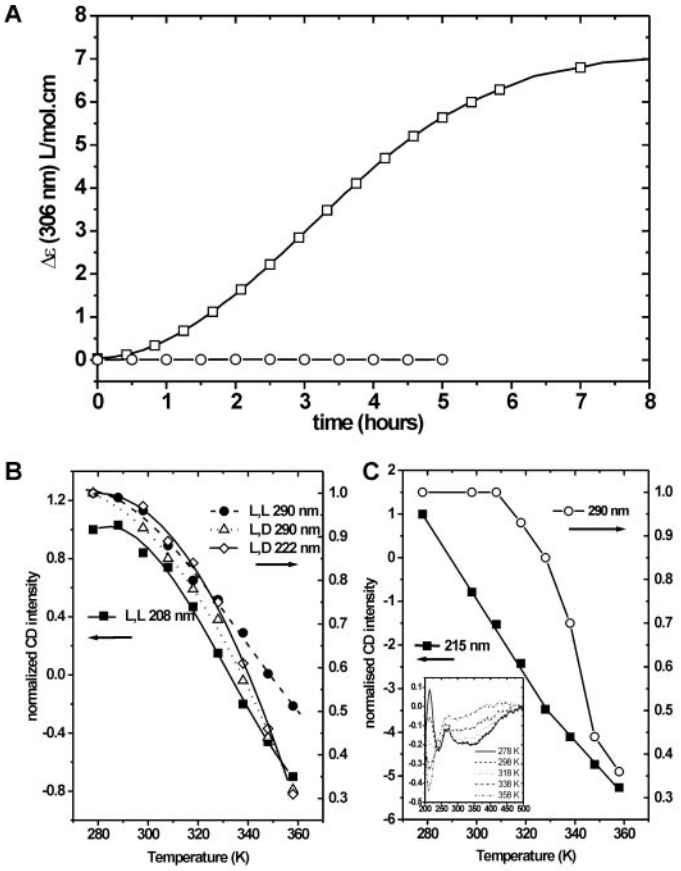

Fig. 4. CD spectral changes in β-helical polymers. (**A**) Acid-catalyzed polymerization of L,L-IAA (○) and L,D-IAA (□) monitored as $\Delta\varepsilon$ (306 nm) versus time. Reaction conditions: 32 mM monomer and 2 μM TFA in dichloromethane at 298 K. (**B**) Temperature dependence of selected CD bands in L,L- and L,D-$(PIAA)_u$ in water. (**C**) Same as (B) for L,L,L-$(PIAAA)_u$; the inset shows the spectra at different temperatures. Sample concentrations were 0.5 mM expressed per repeat unit. After each temperature interval, the solution was equilibrated for 10 min, and a CD spectrum was recorded.

These remarkably defined and rigid, high molecular mass polymers can be considered as synthetic analogs of naturally occurring β-sheet helices, having a related but different β-helix motif. The cooperative behavior of the hydrogen-bonded network in these peptide polymers allows their architecture and thus their properties to be finely tuned. The availability of a large number of natural and unnatural amino acids opens the possibility to design and synthesize a wide array of well-defined β-helical polymers and block copolymers (*23*).

References and Notes

1. M. D. Yoder, N. T. Keen, F. Jurnak, *Science* **260**, 1503 (1993).
2. C. Branden, J. Tooze, *Introduction to Protein Structure* (Garland, New York, ed. 2, 1999).
3. Y.-C. Liou, A. Tocilj, P. L. Davies, Z. Jia, *Nature* **406**, 322 (2000).
4. S. H. Gellman, *Acc. Chem. Res.* **31**, 173 (1998).
5. J. S. Nowick, *Acc. Chem. Res.* **32**, 287 (1999).
6. R. J. M. Nolte, *Chem. Soc. Rev.* **23**, 11 (1994).
7. _____, A. J. M. Van Beijnen, W. Drenth, *J. Am. Chem. Soc.* **96**, 5932 (1974).
8. M. Clericuzio, G. Alagona, G. Ghio, P. Salvadori, *J. Am. Chem. Soc.* **119**, 1059 (1997).
9. M. M. Green, R. A. Gross, F. C. Schilling, K. Zero, C. Crosby III, *Macromolecules* **21**, 1839 (1988).
10. J.-T. Huang, J. Sun, W. B. Euler, W. Rosen, *J. Polym. Sci. Part A Polym. Chem.* **35**, 439 (1997).
11. For a related example in which a helical conformation of a polymer chain is induced and stabilized by dendritic side groups, see V. Percec *et al.*, *Nature* **391**, 161 (1998).
12. See supplementary material on *Science* Online at www.sciencemag.org/cgi/content/full/293/5530/676/DC1.
13. G. C. Pimentel, A. L. McClellan, *The Hydrogen Bond* (Freeman, San Francisco, CA, 1960).
14. D. M. Grant, R. K. Harris, *Encyclopedia of Nuclear Magnetic Resonance*, vol. 4 (Wiley, Chichester, UK, 1996).
15. S. A. Prokhorova, S. S. Sheiko, M. Möller, C.-H. Ahn, V. Percec, *Macromol. Rapid Commun.* **19**, 359 (1998).
16. K. Y. Tsang, H. Diaz, H. Graciani, J. W. Kelly, *J. Am. Chem. Soc.* **116**, 3988 (1994).

17. J. H. K. K. Hirschberg *et al.*, *Nature* **407**, 167 (2000).
18. D. Seebach *et al.*, *Helv. Chim. Act.* **83**, 2115 (2000).
19. B. Baumeister, S. Matile, *Chem. Commun.* **2000**, 913 (2000).
20. C. L. Nesloney, J. W. Kelly, *J. Am. Chem. Soc.* **118**, 5836 (1996).
21. H. L. Schenk, S. H. Gellman, *J. Am. Chem. Soc.* **120**, 4869 (1998).
22. S. R. Griffiths-Jones, M. S. Searle, *J. Am. Chem. Soc.* **122**, 8350 (2000).
23. J. J. L. M. Cornelissen, M. Fischer, N. A. J. M. Sommerdijk, R. J. M. Nolte, *Science* **280**, 1427 (1998).
24. A. L. Spek, *PLUTON. A Program for Plotting Molecular and Crystal Structures* (University of Utrecht, Utrecht, Netherlands, 1995).
25. P. J. H. M. Adams is acknowledged for synthetic contributions, R. P. Sijbesma for help in interpreting the PXRD data, and P. Samori for recording some of the AFM micrographs. This research was supported financially by the Council for Chemical Sciences of the Netherlands Organization for Scientific Research (CW-NWO).

3 May 2001; accepted 21 June 2001

Topochemical Polymerization of C_{70} Controlled by Monomer Crystal Packing

Alexander V. Soldatov,[1]*† Georg Roth,[3] Alexander Dzyabchenko,[4] Dan Johnels,[5] Sergei Lebedkin,[2] Christoph Meingast,[1] Bertil Sundqvist,[6] Miro Haluska,[7] Hans Kuzmany[7]

Polymeric forms of C_{60} are now well known, but numerous attempts to obtain C_{70} in a polymeric state have yielded only dimers. Polymeric C_{70} has now been synthesized by treatment of hexagonally packed C_{70} single crystals under moderate hydrostatic pressure (2 gigapascals) at elevated temperature (300°C), which confirms predictions from our modeling of polymeric structures of C_{70}. Single-crystal x-ray diffraction shows that the molecules are bridged into polymeric zigzag chains that extend along the *c* axis of the parent structure. Solid-state nuclear magnetic resonance and Raman data provide evidence for covalent chemical bonding between the C_{70} cages.

Understanding the formation and properties of three-dimensionally (3D) cross-linked C_{60} (*1–3*) and C_{70} (*4*) requires a detailed knowledge of structure and bonding in their precursors, high-pressure polymerized (hpp) fullerenes (*5–8*). However, with few exceptions (*9–11*), structural studies have been performed on polycrystalline hpp fullerenes, and powder diffraction data are of insufficient quality to resolve individual carbon atom positions and C–C bond lengths of the polymers. In this respect, knowledge of the structure of polymeric C_{70} is particularly interesting because it may be relevant to the not yet understood phenomenon of reversible amorphization induced in this material by high pressure (*12*).

Attempts to produce polymeric C_{70} have generally been inconclusive. Laser desorption mass spectra of thin films irradiated with ultraviolet (UV) light indicated the presence of molecular clusters, although infrared (IR) spectra remained unchanged (*13*). High-pressure treatment of C_{70} powder up to 7.5 GPa at temperatures up to 800°C also did not change its structure and vibrational properties (*14*). New features in IR (*15, 16*) and UV–visible (*15*) absorption spectra of polycrystalline C_{70} were observed after treatment at 5 GPa, 300°C (*15*) and 7.5 GPa, 250°C (*16*), but these features were attributed to the formation of C_{70} dimers, which were later produced, isolated in pure form, and characterized spectroscopically (*17*). However, the crystal structure of C_{140} also remains unknown. All of these uncertainties have frustrated further attempts to access the polymeric state of C_{70} and to address the problem of C_{70} polymerization in general.

To guide our experimental studies, we generated a series of plausible structural models for polymeric C_{70} (Table 1) using rigid zigzag chains as the structural units. We rejected some "hypothetical" polymeric structures from the analysis as energetically unrealistic, such as a fivefold helix extended along the ⟨111⟩ direction in a crystal with cubic packing (CP) or chains formed in close-packed planes via 2+2 cycloaddition between "equator" double bonds of C_{70}. For comparison, we also constructed crystal structures based on rigid, energetically favorable C_{140} (C_{2h} symmetry). The molecular structure as well as the initial packing [either CP or hexagonal packing (HP)] were assumed to be similar to that in a monomer (*18–21*). The positions and mutual orientations of chains and dimers were then optimized via minimization of the lattice energy with a method (*22*) that successfully predicted the crystal structures of monomeric C_{60} and C_{70} and of polymeric C_{60}. The predicted structures (Table 1) show that, whereas dimers can be formed in either packing, a polymeric chain structure with a reasonably low free energy is possible only in hexagonal C_{70}, because CP does not have a symmetry element (twofold screw axis) required to build a polymer. We therefore decided to use a HP C_{70} single crystal as source material for high-pressure synthesis of a C_{70} polymer. The predicted polymeric structures were further used as starting models in the structure determination from our diffraction data (see below).

The single crystals of C_{70} were grown with a method described in (*23*) and were treated

Table 1. Predicted and observed crystal packings of C_{70} polymer and dimer (*26*). The observed monomer structure is from (*21*), *Z* is the number of fullerenes per unit cell, and the van der Waals lattice energy (per one C_{70}) was minimized with the Lennard-Jones 6-12 atom-atom potential with parameters r_0 = 3.7 Å, ε = −0.072 kcal/mol for carbons using the program PMC (*22*). ND, not determined.

	Monoclinic dimer	Trigonal dimer	Orthorhombic polymer	Hexagonal polymer	Observed polymer	Observed monomer
Space group	*C*2/*m*	$P3_1$	*Ccmm*	$P6_3/mcm$	*Ccmm*	*Pnam*
Z	4	6	4	6	4	4
Crystal packing	HP	CP	HP	HP	HP	HP
Lattice energy (kcal/mol)	−43.3	−42.8	−60.90	−51.64	ND	ND
Density (g/cm^3)	1.844	1.835	1.916	1.736	1.804	1.733
Lattice parameters						
a (Å)	16.93	9.97	16.95	18.13	17.30	17.35
b (Å)	10.06	9.97	10.13	18.13	9.99	9.84
c (Å)	17.86	53.01	16.97	16.97	17.92	18.34
α (degrees)	90	90	90	90	90	90
β (degrees)	84.3	90	90	90	90	90
γ (degrees)	90	120	90	120	90	90

[1]Institut für Festkörperphysik, [2]Institut für Nanotechnologie, Forschungszentrum Karlsruhe–Technik und Umwelt, Post Office Box 3640, D-76021 Karlsruhe, Germany. [3]Institut für Kristallographie der Rheinisch-Westfälische Technische Hochschule Aachen, Jägerstrasse 17–19, D-52056 Aachen, Germany. [4]Karpov Institute of Physical Chemistry, 103064 Moscow, Russia. [5]Department of Chemistry, [6]Department of Experimental Physics, Umeå University, S-901 87 Umeå, Sweden. [7]Institut für Materialphysik, Universität Wien, A-1090 Wien, Austria.

*Present address: Department of Physics, Lyman Laboratory, Harvard University, Cambridge, MA 02138, USA.
†To whom correspondence should be addressed. E-mail: soldatov@physics.harvard.edu